Journal of
Ceramic Science
and Technology

Degradation of Sealing Glasses for SOFC under Electrical Load and Dual Atmosphere

A. Rost[*], J. Schilm, M. Kusnezoff, A. Michaelis

Fraunhofer Institute for Ceramic Technologies and Systems, Winterbergstrasse 28, 01277 Dresden, Germany

Abstract

For reliable operation of planar solid oxide fuel cells (SOFC), long-term stability of the sealing materials, including gas tightness and bonding to the joined materials, is essential. Failures induced by thermal cycling, slight stack deformation or degradation of the sealing material can lead to leakages and undesired combustion of fuel gas, causing hot spots and severe damage of stacks or whole systems. Suitable partially crystallizing SOFC sealing glasses are presented and characterized in terms of their softening properties, viscosity, thermal expansion and crystallization behaviour. However, it is not sufficient to characterize these internal properties. For reliable long-term operation, structural changes of sealing glasses and particularly reactions between interconnector materials and sealing glasses have to be considered. Therefore model sealings are tested in dual atmospheres with applied voltage. The resistivities of these arrangements were monitored continuously and changes in the microstructure of the joints were investigated after testing. The results are discussed in terms of the devolution of resistivity of model sealings at high temperatures and the microstructures of the sealing glasses and the glass-to-metal interfaces. After the identification of critical glass components, the development of enhanced sealing glasses with improved degradation properties is demonstrated and shown for one composition.

Keywords: Crystallization, degradation, sanbornite, sealing glasses, SOFC

I. Introduction

SOFC systems based on planar stack designs are currently being developed for a broad range of mobile and stationary power sources. For these stack designs, sealings are a critical issue. Situated in the high-temperature parts of the stacks, they have to withstand temperatures up to 800 – 900 °C for up to 40 000 h. Sealings have to separate fuel gas from air in the system and ensure the mechanical integrity of the arrangement of stack components. For this reason, the sealing materials have to be chemically stable at high temperatures against harsh gaseous environments and the joined materials. Furthermore, the seals between adjacent metallic interconnectors have to provide electrical insulation in the stacks. Depending on the SOFC design, it is possible that sealings are exposed to voltages typical for single cells, but also to high voltages produced by whole stacks.

Under the operating conditions of SOFCs, glass is a chemically very stable and compatible sealing material. It has the advantages of being an electrical insulator, cheap to produce on a large scale and easy to apply in a variety of shapes if prepared as tapes or pastes. Different compositions of sealing glasses are widely discussed in the relevant literature [1−6]. Most of these publications address the intrinsic properties of the glasses, such as their thermal expansion coefficients, crystalline phases, viscosity or resistivity. However, for joining and sealing of SOFCs, not only these properties of the sealing material are important. Only a few authors consider the fact that seals must exhibit long-term stability against the sealed materials under very aggressive conditions in order to achieve gas-tight joints. In SOFCs such materials are mainly high chromium-alloyed steels, nickel-based alloys or sinter metals [7, 8]. Virtually no literature is known which addresses the long-term stability of glass seals in contact with metallic interconnectors under operating conditions including the effects of high temperatures, dual atmospheres and electric potentials to which the sealed components are exposed. It is generally accepted that the reactivity of glass with ceramic components like MEAs made of doped ZrO_2 is much less pronounced than with metallic interconnector materials, e.g. Crofer 22 APU. An electric potential applied across the seals will additionally influence the reactivity between the metallic substrates and sealing glasses at high temperatures. Under SOFC operating conditions, partially crystallized sealing glasses contain a fraction of a highly viscous glass melt above the glass transition temperature T_g. At temperatures above T_g, the mobility and reactivity of glass components are increased by several orders of magnitude in comparison to solid glasses at ambient temperatures. An electric field will force the migration of mobile ions in this glass melt, leading to polarization effects in the glass and also at the glass-to-metal interfaces. Additionally, voltage can contribute to interdiffusion of ions from the metals components into the glass and vice versa; redox re-

* Corresponding author: axel.rost@ikts.fraunhofer.de

actions between glass and metals also have to be taken into account.

The main part of the presented study is focused on interfacial reactions between metallic interconnector materials and partially crystallized sealing glasses under conditions typical for the operation of SOFC systems. The direct testing of sealing glasses in real SOFC stacks is associated with several disadvantages. First of all, stacks are expensive and, as a consequence, testing of glasses would also be so. Furthermore, SOFC systems often do not operate under reproducible and stable testing conditions. But also parameters like testing times, gas composition and flow, thermal cycling and produced current can vary within one single stack test and even more often when series of stacks are tested. Therefore, the results of post mortem analysis of stacks provide valuable information on sealing glasses, but data from different stacks are often not comparable. Therefore, a unique testing furnace for operating with dual gas atmospheres up to 1 000 °C was developed which is capable of hosting four model sealings simultaneously. The samples can be independently impinged with varying fuel gas compositions and electric potentials up to 30 V. In contrast to real stacks, the resistivities of the sealed arrangements are directly measured during the testing procedures. The need for potentials as high as 30 V strongly depends on stack designs where sealing glasses sometimes do not only have to withstand single cell voltages of 0.7 – 1.3 V but also the potential of the whole stack. The setup of the model sealing and its integration in the test system is depicted in Fig. 1; further information is available in [9]. The devolution of the resistivity accompanied with SEM investigations of cross-sections provides information for the understanding of degradation processes in the glasses as well as at the glass-to-metal interfaces, and for an improvement of sealing glasses.
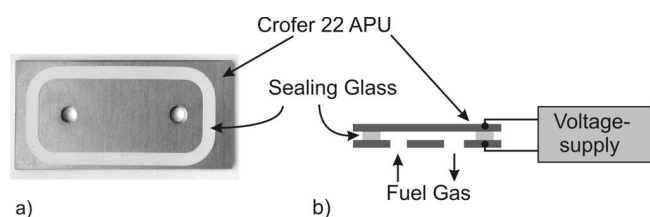
Fig. 1: a) Top view of model seals, made of glass paste on a Crofer 22 APU- substrate b) Schematic drawing of the measuring setup. The inner part of the sample is flushed with fuel gas and air is at the outer side.

II. Experimental

A number of partially crystallizing glasses from the system $BaO-Al_2O_3-SiO_2$ with molar SiO_2: BaO ratios close to 2, containing B_2O_3 and further additives such as ZnO and other oxides in amounts of less than 10 mol%, have been selected for this study. The glasses contain sanbornite ($BaSi_2O_5$) as the main crystalline phase, which is necessary to adjust the coefficient of thermal expansion for matching the values of YSZ and Crofer 22 APU. The ZnO-containing glass (S01) represents a standard sealing glass which is commercially used for joining and sealing of SOFC based on Crofer 22 APU interconnectors (staxera, Dresden). With S02 a newly developed sealing glass is present-

ed, which is free of ZnO oxide. A quaternary $BaO-Al_2O_3$-$SiO_2-B_2O_3$ glass (M01) is used as a model glass to show the necessity of controlled crystallization processes in partially crystallizing sealing glasses. The overall composition of this model glass is maintained with respect to the other glasses.

All glasses were molten from the reagent grade raw materials in platinum crucibles at 1 500 °C for 1 h. After melting, the glasses were fritted by pouring them into cold water, dried at 150 °C for 5 h and ground to powders with $d_{50} < 10 \mu m$. The characterization of glass powders included several relevant properties to evaluate the conditions for the sealing processes. Thermal expansion was measured from crystallized powder compacts in a horizontal pushrod dilatometer "DIL 402 E" from "NETSCH Gerätebau GmbH". The coefficient of thermal expansion (CTE) is stated as the technical expansion coefficient, where the thermal expansion is referred to room temperature.

The shrinking and softening properties were observed by means of hot stage microscopy (HSM) using a "Leica Hot Stage Microscope". Crystalline phases were determined with Rietveld analysis after appropriate thermal treatment of the glass samples according to sealing processes of SOFC stacks. Additionally, thermal analysis by means of DSC (NETZSCH DSC 404 F1) was conducted to determine crystallization temperatures.

For the preparation of the model sealings, pastes for screen-printing processes were prepared. Multiple screen-printing of the pastes was conducted on Crofer 22 APU substrates having lateral dimensions of 30 x 60 mm² and a thickness of 2.5 mm as shown in Fig. 1a. Sandwich-type samples were prepared by stacking two of these coated substrates where one substrate was provided with two holes for realizing a continuous gas flow inside the closed samples (Fig. 1 b). After sealing, the glass joints had a constant height of 250 μm, realized by ceramic spacers placed between the metallic substrates, and a wideness of 3.5 to 4 mm. Heat treatment for the sealing process was chosen according to the softening and the crystallization properties of the glasses.

These model sealings were tested at 850 °C in a dual atmosphere with simultaneous application of a d.c. voltage ranging from 0.7 V up to 30 V. Values for resistivity are obtained by measuring the electric current and regarding the geometry of the joints. Owing to the application of a d.c. potential, an electric field with a given direction is formed across the sample and, as a consequence, the glass-to-metal interfaces are constantly polarized in one way. In electrochemical terms, one interface is polarized as a cathode (reducing conditions) and the other interface as an anode (oxidizing conditions). This nomenclature refers to the type of electrochemical polarization of the substrates but not to the usually known "anodic" and "cathodic" side of fuel cells. For the fuel gas atmosphere, a gas composition by volume of 30 % H_2; 7 % CO_2; 3 % $H_2O_{(g)}$ and 60 % N_2 was chosen. Before and after testing, the gas tightness of the samples is measured in helium leak tests. Leakage rates lower than 10^{-8} mbar l s^{-1} cm^{-1} were accepted for sufficient gas-tight samples. The microstructure of the joints
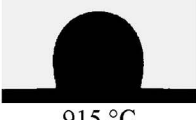
was examined on polished cross-sections with scanning electron microscopy (SEM) in the back-scattered electron (BSE) contrast mode and with energy-dispersive X-ray spectroscopy analysis (EDX).

III. Results

(1) Characterization of sealing glasses

The sintering and softening properties can be well characterized with hot stage microscopy. This method enables *in situ* measurement of sintering processes of the powder compacts along with calculation of the shrinkage. In addition, the viscosity of amorphous materials can be determined at certain temperatures based on the shape of the samples. The values of these viscosity fix-points are widely discussed and reviewed in the literature [10–13]. Fig. 2 shows the linear shrinkage of all three glasse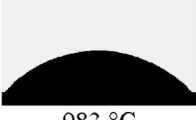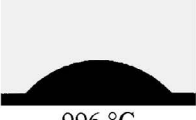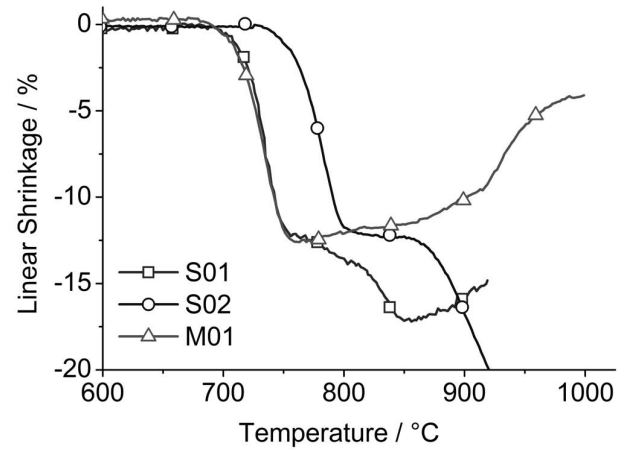s as a function of temperature (heating rate of 5 K/min in air on YSZ substrates). While the sealing glasses S01 and S02 show a viscous flow and further shrinkage – owing to wetting of the substrates after reaching their maximum sintering density – the model glass M01 continuously expands at temperatures above 760 °C.

Fig. 2: Sintering properties and viscous flow of the glasses measured by means of hot stage microscopy (HSM) at a heating rate of 2 K/min in air.

Additionally, it is shown that the sintering process of the sealing glass S02 is shifted towards higher temperatures in comparison to S01 and M01. Table 1 lists characteristic changes of the shapes of the cylindrical samples which were deduced from the HSM measurements together with the viscosity fix-points found in the literature.

Table 1: Images of characteristic changes in shape of cylindrical glass powder compacts during heating in a hot stage microscope in air.

	Sealing glass S01	Sealing glass S02	ZnO-free model glass M01
Begin of sintering (10^9 Pa·s)	691 °C	736 °C	692 °C
End of sintering (10^7 Pa·s)	749 °C	818 °C	755 °C
Softening point ($10^{5.5}$ Pa·s)	777 °C	832 °C	not detected (900 °C)
Ballpoint ($10^{4.5}$ Pa·s)	915 °C	884 °C	not detected (930 °C)
Halfball ($10^{3.5}$ Pa·s)	931 °C	912 °C	not detected (960 °C)
45°-Angle ($10^{2.2}$ Pa·s)	983 °C	996 °C	not detected up to 1000 °C

While the sealing glasses S01 and S02 show softening properties which are almost typical for glasses, the model glass M01 shows no additional dimensional changes during the sintering process.

This model glass shows a strong crystallization process occurring during or even at the end of the sintering process. According to Fig. 2, the overall sintering shrinkage of M01 is comparable with S01 and S02, and therefore the crystallization does not seem to affect the sintering process. In the sintered glass M01 the crystallites must form a skeleton which stabilizes the microstructure to prevent softening of the partially crystallized glass and wetting of the substrate. Owing to this strong and early crystallization, the model glass M01 is not suitable for sealing applications. In case of S01 it has to be mentioned that the so-called "ball point" is not ideally shaped, which can also be explained based on the crystallization process.

A closer view of the different viscosities of the glasses is provided by plotting the viscosity against the temperature. Therefore the six viscosity fix-points listed in Table 1, ranging from the start of sintering with $\eta = 10^9$ Pa·s to the 45°-angle (Flow point) with $\eta = 10^{2.2}$ Pa·s are used as seen in Fig. 3. Additionally the Transformation Temperature (T_g) obtained with CTE plots of Fig. 7 with $\eta = 10^{12}$ Pa·s is included. While the glass S02 shows a nearly continuous decrease in viscosity with temperature, the glass S01 offers a step in the range of 760 – 950 °C. It can be assumed that the crystallization process is responsible for the inhibited softening before the ball point is reached. For the glass M01 it is only possible to use the T_g value from CTE measurements as well as the start and the end of the sintering process. It is seen that up to a temperature of 840 °C the sealing glass S02 shows a higher viscosity than the glass S01.
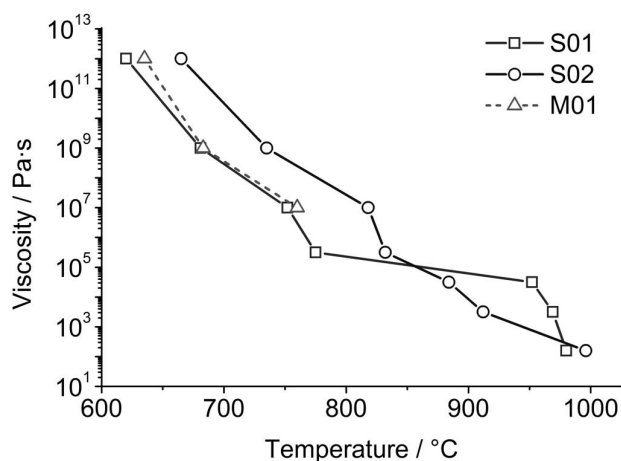

Fig. 3: Plot of viscosity fix-points (measured with HSM) and T_g (CTE analysis Fig. 7) of the S01 and S02 glasses versus the temperature.

In order to reveal more information on the crystallization processes, DSC analysis of all glasses has been conducted. Despite the fact that the results gave less featured plots some details can be deduced in relation to the HSM data (Fig. 4). For the measurement it was necessary to conduct a second measurement for the baseline correction. Owing to the fact that this was done with a second heating of

each sample, the glass transition temperatures, which are normally seen in such DSC analysis, are not visible.
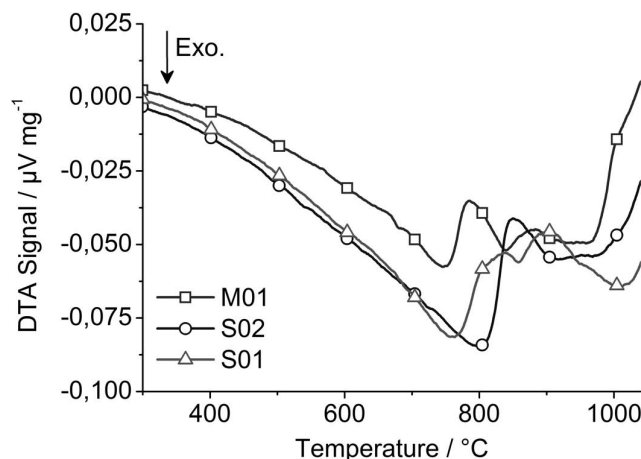

Fig. 4: Comparison of DSC results of the different glasses measured at 5 K/min in air.

A graphical superposition of the HSM and DSC plots of the sealing glass S01 is given in Fig. 5. HSM analysis shows that the sintering process, which ranges from 680 – 750 °C, concurs well with the shoulder of the DSC data, which is located in the same temperature range. According to Eberstein *et al.*, the shoulder in the DSC plot results from an increasing heat transfer into the sample owing to reduced porosity of the compacted sample [13]. A smooth exothermic peak at 780 – 820 °C was detected, which can be attributed to a crystallization process. This supports the formerly made assumption that crystallization inhibits the softening of the glass S01. The DSC results of S02 and M01 also show sintering shoulders and weakly pronounced crystallization peaks (Fig. 4). In the case of the model glass M01, the DSC data show a two-step sintering process which overlaps with a small crystallization peak. This suggests that the endothermic sintering shoulder and the exothermic crystallization signal are superimposed and are so not clearly detectable.
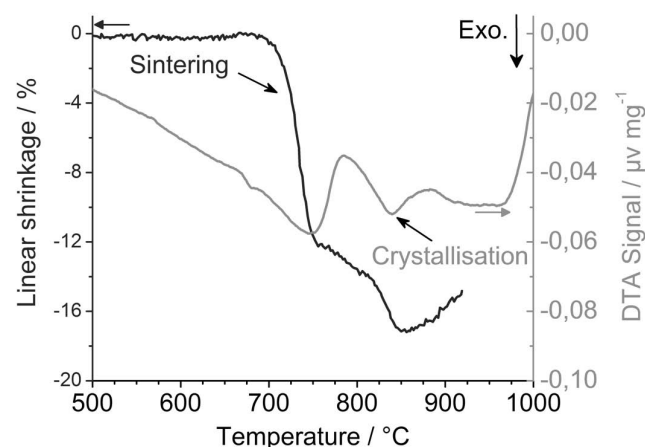

Fig. 5: Comparison of DSC and HSM results of the S01 glass measured at 5 K/min in air.

For quantitative measurements of the crystalline phase contents, samples of all glasses were heat-treated according to a thermal profile typical for the sealing of SOFCs in-

cluding a sealing process and a crystallization time of 30 h at 850 °C in air. Results of Rieveld analysis indicate sanbornite (low-temperature modification of $BaSi_2O_5$) as the main crystalline phase for all glasses (Table 2). Despite similar SiO_2 : BaO ratios as well as similar Al_2O_3 and B_2O_3 contents, the data show that the model glass M01 contains a significantly higher content of $BaSi_2O_5$ than S01. This supports the formerly made assumption concerning the DSC and HSM results of the glass M01. This in turn explains the necessity of an additional component (ZnO for the sealing glass S01) for controlling and limiting the crystallization velocity. This is also confirmed with the results of Capoglue *et al.* [14]. In the case of S02, ZnO has been replaced with a corresponding amount of an alternative oxide. Here, the crystallization of $BaSi_2O_5$ is reduced and a small amount of cristobalite (SiO_2) is detected. Fig. 6 shows the corresponding XRD diffractograms of the samples.

Table 2: Contents of crystalline phases in sealing glasses after heat treatment according to a typical joining profile for SOFC stacks, measured by means of Rietveld analysis with alumina as internal standard.

| Glass	$BaSi_2O_5$ (LT-type)/wt%	SiO_2 (cristobalite)/wt%
S01	25 ±2	none
S02	20±2	< 2

The technical coefficient of thermal expansion (CTE) is shown in Fig. 7 for crystallized samples of all glass ceramics. The scattering of the data is about ±4 % of the measured value. Having the highest content of $BaSi_2O_5$, the model glass M01 shows the highest coefficient of thermal expansion. Unfortunately, this glass is not suitable for sealing processes owing to an insufficient softening behaviour. In contrast to this, S01 has a slightly lower CTE and shows softening at temperatures that are appropriate for SOFC sealing processes. In the case of the glass S02, a phase transformation of cristobalite at temperatures of 220 – 300 °C causes a discontinuity as seen for the plot of the corresponding CTE-data. According to the HSM results, the glass transition temperature (T_g) of S02 is, as compared to S01 and M01, also shifted to higher temperatures by 50 K.

The results show that the intrinsic properties of the partially crystallizing glasses S01 and S02 are suitable for their application as sealing glasses for SOFC. But these data do not allow any predictions concerning their long-term stability under conditions that are typical for the operation of SOFCs.

(2) Interactions of sealing glasses with Crofer 22 APU under electrical load

In a first set of experiments, four model sealings based on the glass ceramic S01 were exposed for 500 h in dual atmosphere at 850 °C with an applied voltage of 0.7 V. Fig. 8 shows the measured currents of each sample recalculated as resistivities. All samples were treated with the same time-temperature profile in the furnace, but the starting

times for applying the electric potential were varied. This means that sample A was exposed to the electric potential for the whole time of the experiment. For the samples B, C and D the voltage was applied after 50, 100 and 200 h of exposure at 850 °C in the dual atmosphere.
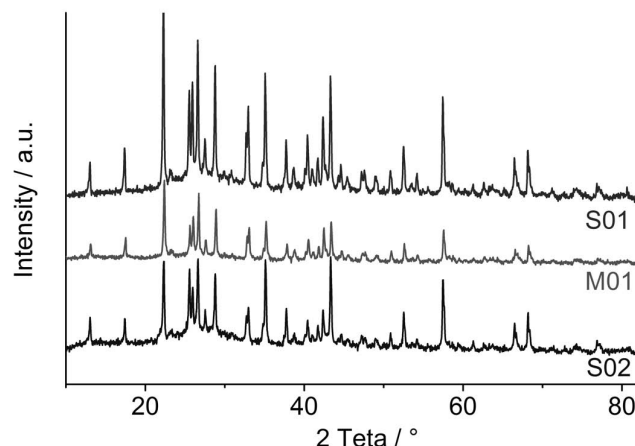
Fig. 6: XRD diffractograms of crystallized glasses; low-temperature modification of $BaSi_2O_5$ is identified as the only crystalline phase.
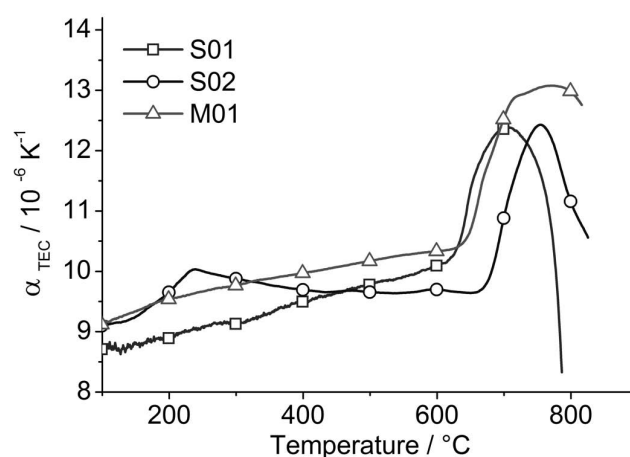
Fig. 7: Technical expansion coefficient of crystallized glasses.
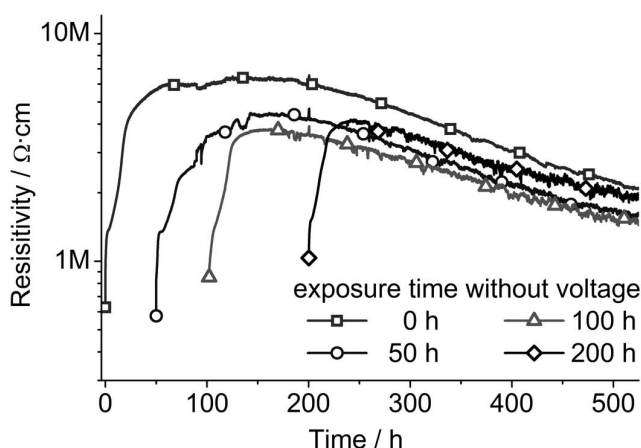
Fig. 8: Resistivities of glass joints at 850 °C in dual atmosphere. Voltage of 0.7 V was applied at 0, 50, 100 and 200 h after starting the test at 850 °C. Consider the logarithmic scale of the diagram.

The plot of the resistivity of sample A can be taken as characteristic and is explained in detail. Initially, a strong increase of the resistivity within the first 50 h of testing occurs. It is assumed that this is caused by polarization effects in the viscous glassy phase. At 850 °C, ions in the glass have mobility, high enough to migrate in the electric field. Two kinds of ions are thought to migrate: barium or oxygen ions. According to [15, 16], mainly barium ions are able to migrate in the glass. But also oxygen ions may contribute to the conductivity. For both kinds of ions having the same mobility, it is hard to decide whether oxygen or barium ions mainly contribute to the conductivity [17] or even both. After an initial increase, the resistance reaches nearly a constant level for a period of about 100 h. Afterwards, the resistivity of the sample A continuously decreased with time, not reaching a constant level even after 500 h of testing. This behaviour denotes an increasing electric current, which in turn can be interpreted as compositional changes of the glass itself, reactions at the glass-to-metal interfaces or also as reactions of the glass with the atmospheres. In former investigations, it was found that a reducing atmosphere has only a minor influence on the development of the resistivity [18].

A similar behaviour of the resistivity as seen for sample A can be found for the samples B to D when voltage is not applied immediately after a temperature of 850 °C is reached but after the samples have been exposed to this temperature for 50, 100 or 200 h. However, within this series sample A shows the highest resistances from the beginning to the end. All other samples show lower resistivities but the same characteristic and the all resistivities decrease with similar rates (consider the logarithmic scale of the diagram in Fig. 8). After 500 h of testing, the measured resistivities range within 1.5 and 2.1 MΩ·cm. In order to get an indication of the accuracy of the *in situ* resistivity measurements, we refer to Fig. 14 where two different measurements, each with a retake, are presented.

SEM analyses of the interfaces between the sealing glasses and Crofer 22 APU from selected samples in Fig. 8 before and after testing provide an insight into microstructural changes in the sealing glass and especially at the glass-to-metal interfaces. In Fig. 9 a. the conditions direct after joining are shown, without the application of any voltage. There are no differences between the two glass-to-metal interfaces. Between glass and Crofer 22 APU, a $3-5$ μm thick intermediate layer has been formed. EDX analyses reveal an oxidic composition of this layer with silicon, barium and chromium as the main components. This layer is formed by surface oxidation of the Crofer 22 APU and interaction with the glass phase under sealing conditions. The microstructure of the glass shows a few pores and homogeneously distributed $BaSi_2O_5$ crystals with diameters of a few micrometers. After the samples are exposed to high temperatures with an applied voltage of 0.7 V across the sandwich-type samples, the opposed polarized interfaces differ markedly. Figs. 9 b and c show cross-sections of the samples A and D with the annotations according to the polarization. At cathodically polarized glass-to-metal interfaces, EDX analyses reveal the formation of a Cr-Mn-oxide layer [19]. In contrast to the known oxide layer of uncovered Crofer 22 APU, this oxide layer is enriched with zinc, a component of the glass. EDX analysis reveals differing amounts of the single elements, so that a composition of $(ZnCrMn)_3O_4$ is assumed. Additionally the surface of the Crofer 22 APU also seems to be rougher in comparison to the as-joined state.
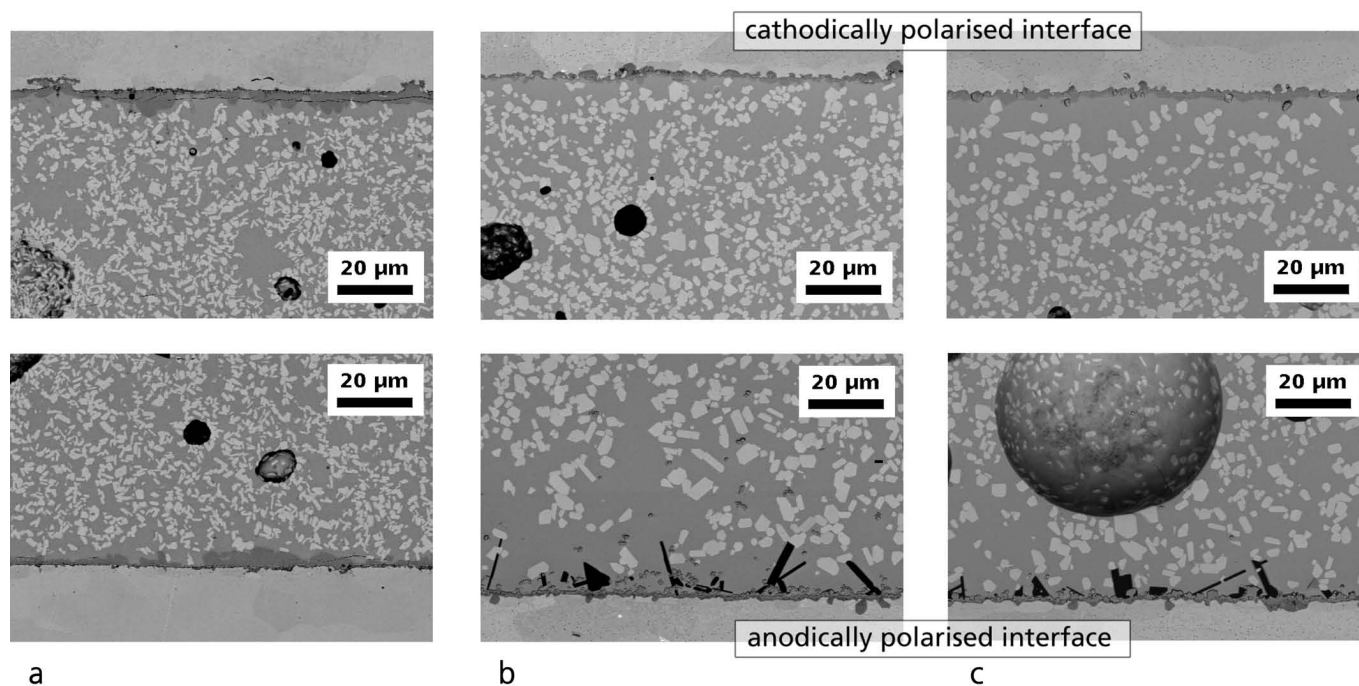

Fig. 9: Interfaces between Crofer 22 APU and sealing glass. The interfaces are denoted as cathodic for reducing and anodic for oxidizing conditions. a) Microstructure after joining of the samples (no additional treatment) b) Voltage applied after reaching 850 °C (sample A of Fig. 8) c) Voltage applied after 200 h dwell time at 850 °C (sample D of Fig. 8)

At anodically polarized interfaces, the composition of the $1 - 3\,\mu$m-thick oxide layers has been changed considerably. EDX analysis revealed an oxide layer again consisting of $(ZnCrMn)_3O_4$. Furthermore, single particles with a similar composition to this oxide layer have migrated in the glass matrix (dark grey) as seen in the lower image of Fig. 9 b. Additionally, at all anodically polarized interfaces crystalline SiO_2 needles are detected adjacent to the oxide layer (black appearance in the BSE contrast in Figs. 10 b and c). As seen at the cathodically polarized interfaces, the surfaces of the Crofer 22 APU substrates show a rough structure, indicating a slightly proceeding destruction of the microstructure. Regarding the glass phase itself, a grain coarsening of the $BaSi_2O_5$ crystals has occurred in the case of both samples A and D after 500 h at 850 °C.

These results show that interfacial reactions between the sealing glass and Crofer 22 APU influenced by the type of polarization of the metallic substrates can be referred to the applied electric potential. Neither changes in the microstructure of the glass nor strong growth of interfacial layers can be taken as explanations for the continuous decrease of resistivities. It seems to be more probable that the structural changes in the interfacial layers are responsible therefore. The consumption of electric charge owing to redox reactions between Crofer 22 APU and the sealing glass leads to an increased current. The migration of oxidic particles at the anodically polarized interfaces can also contribute to this effect.
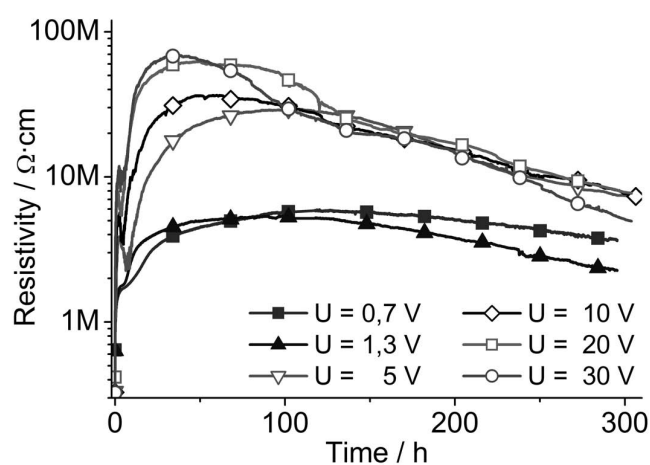

Fig. 10: Resistivities of glass joints at 850 °C in dual atmosphere at voltages between 0.7 and 30 V. Consider the logarithmic scale of the diagram.

To clarify the effect of externally applied potential on the resistivities, samples were treated with higher electric potentials up to 30 V. The plots of the resistivities are shown in Fig. 10. The devolution of the resistivities of the 0.7 and 1.3 V samples are comparable with the data shown in Fig. 9. For higher voltages, the resistivities are shifted to much higher values and reach their maximum after shorter testing times. For the 30 V sample, a peak resistivity of 68 MΩ·cm is reached after 34 h. With increasing values of the voltage, the peak resistivities are more sharply pronounced. This behaviour can be attributed to stronger polarization and charge separation at the glass-to-metal interfaces and also in the glass structure for increasing potentials. Additionally, with increasing voltages the resistivities tend to decrease with higher rates (Consider the logarithmic scale).

Fig. 11 compares anodically and cathodically polarized glass-to-metal interfaces of samples treated with 0.7, 5 and 30 V according to the results shown in Fig. 10. At the anodically polarized interfaces the formation of SiO_2 needles on top of the $(ZnCrMn)_3O_4$ layer is detected again. In case of the 0.7 V sample, only some single crystals have been formed and also $(ZnCrMn)_3O_4$ particles have migrated into the glass phase. By applying higher voltages, dense layers of SiO_2 crystals are formed at anodically polarized interfaces. In these cases, no $(ZnCrMn)_3O_4$ particles are detectable. The SiO_2 layers seem to have a barrier function that hinders the separation and migration of particles from the $(ZnCrMn)_3O_4$ layer. Owing to the inhomogeneous structure of this layer, no clear differences between 5 V and 30 V samples can be identified. However, in contrast to the 0.7 V and 5 V samples, the $(ZnCrMn)_3O_4$ layers of the 30 V sample become much more porous and roughly structured. The attack and destruction of the Crofer 22 APU surfaces also becomes stronger with increasing potentials.

At cathodically polarized interfaces, structured oxide layers are found. Besides their main components (BaO, SiO_2 and Cr_2O_3), they also contain manganese oxide and zinc oxide. The thickness of the layers increases with the applied voltage and the surface of the Crofer 22 APU shows pores beside the oxide layer together with an increasing roughness. For voltages from 5 V, metallic particles with compositions similar to the Crofer 22 APU are also detected within these layers. Additionally, metallic inclusions of zinc with minor amounts of iron can be detected next to the oxide layer in the glass structure.

As shown in Fig. 12, the higher voltage also leads to the formation of large pores in the bulk structure of the composition S01. Measurements of very high helium leakage rates for model sealings treated with high electric potentials confirm the destructive effect of these large pores. Fig. 13 shows the helium leakage rates measured on the samples in Fig. 10. Owing to the severe damage to the sealing glasses with open channels in the bulk structure, voltages higher than 10 V result in leakage rates higher than 10^{-8} mbar l s^{-1} cm^{-1}. So they do not meet the commonly accepted gas tightness for sealings in SOFC applications of less than 10^{-8} mbar l s^{-1} cm^{-1}.

From the compositions of the interfacial layers it turns out that in all cases ZnO is involved in the formation of these layers and the migration process of oxidic particles observed at lower voltages. Under certain conditions metallic zinc inclusions are also formed (Fig. 11). Hence, it can be assumed that the replacement of ZnO by suitable non-reactive components in the used glass ceramic seals can lead to enhanced stability in contact with Crofer 22 APU interfaces. With the model glass M01 it has been shown that a simple elimination of ZnO in the composition of the sealing glass S01 leads to fast crystallization of the glass ceramics. This in turn leads to unsuitable properties for sealing applications in SOFC stacks. Thus, ZnO has to be replaced by other components which ideally affect the crystallization velocity of the glass during the sealing process but do not participate in degradation processes between the glass ceramic and the metallic interconnector materials or even in the crystallization process by possibly leading to undesired crystalline phases.
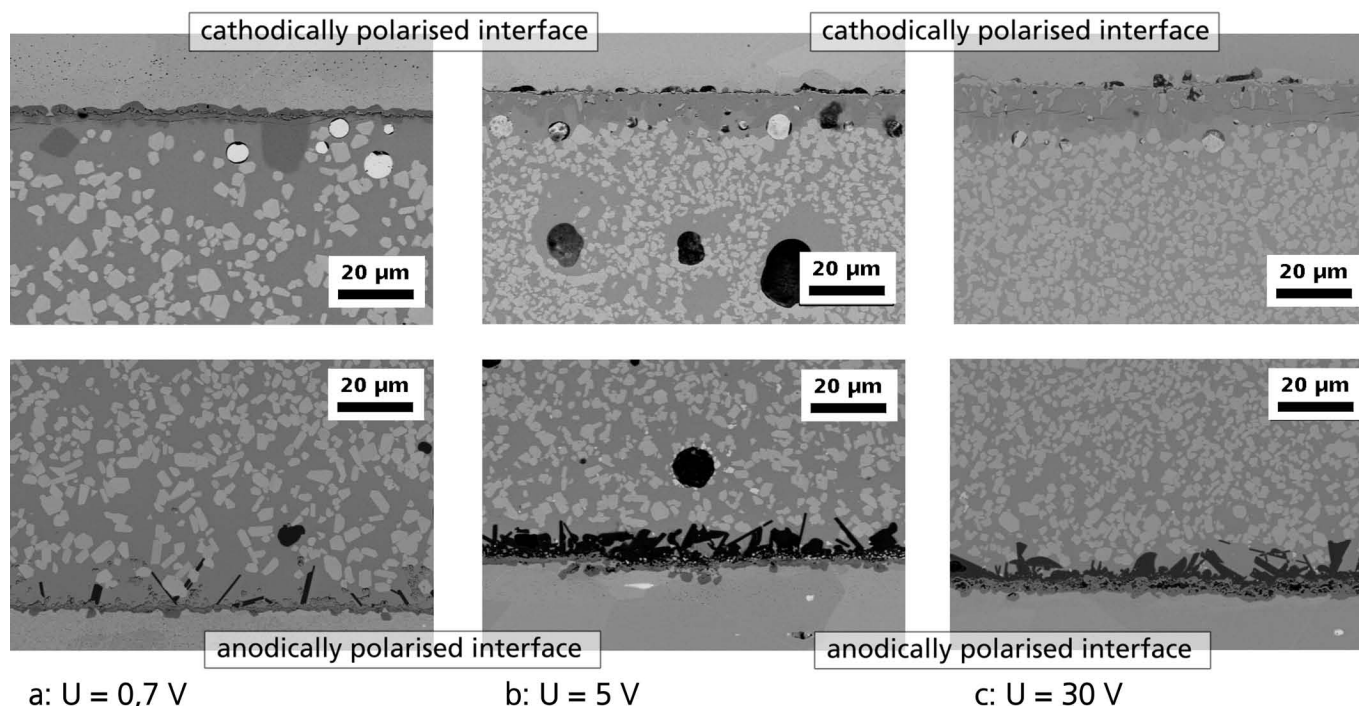
Fig. 11: Interfaces between Crofer 22 APU and sealing glass after 300 h at 850 °C with different voltages. The upper images present the cathodic conditions and the lower ones the anodic conditions..
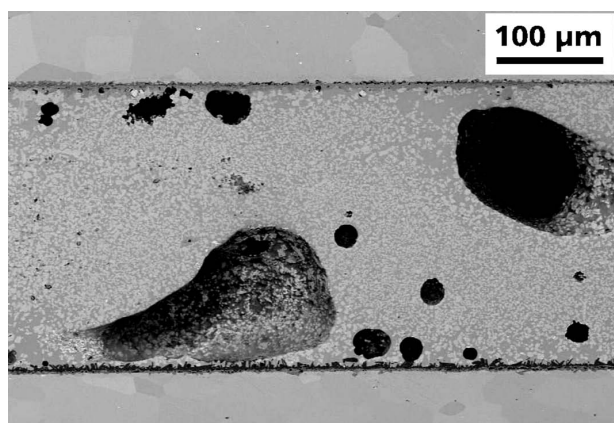

Fig. 12: Microstructure of the S01 sealing glass after exposure to 850 °C for 300 h with an applied voltage of 30 V.

The composition S02 presented in this work is a result of the development of sealing glass ceramics for SOFC with enhanced stability against degradation effects. It is free of ZnO, shows controlled crystallization properties and is therefore suitable for sealing processes of SOFC (cf. 3.1). Fig. 14 shows the resistivities of model samples manufactured with the sealing glass S02 tested in dual atmosphere at 850 °C with an applied voltage of 0.7 V and 30 V. For 0.7 V the resistivities reach a level of around 10 MΩcm, which fluctuates slightly with time. However, no continuous decrease in resistivities occurs as it is observed for ZnO-containing sealing glasses. When a voltage of 30 V is applied, the devolution of the resistivity is similar to that observed for the sealing glass S01. It is worth pointing out that both measurements show a good repeatability and a quite low scatter with respect to the measured values in the MΩ-range.
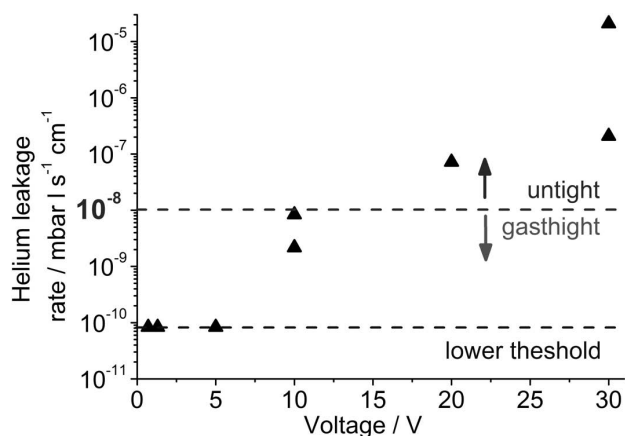

Fig. 13: Helium leakage rates of model sealings after exposure to dual atmosphere at 850 °C for 300 h with different electric potentials applied.
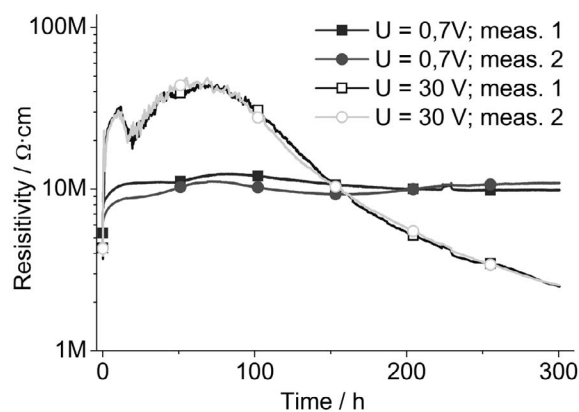

Fig. 14: Resistivities of an optimized ZnO-free sealing glass (S02) in dual atmosphere at 850 °C with applied voltages of 0.7 and 30 V, each measurement is conducted on two samples. Consider the logarithmic scale of the diagram.

Cross-sections of these model sealings were investigated with SEM. An overview of the microstructure of samples treated with 0.7 V and 30 V including both interfacial regions is presented in Fig. 15.

According to the XRD results in Table 2, after crystallization the ZnO-free glass ceramic contains small amounts of cristobalite. This phase is formed *in situ* during the crystallization processes even when no voltage is applied to the glass and the glass is not in contact with Crofer 22 APU substrates. In Fig. 15 the cristobalite phase is represented as small irregularly formed and dark crystals throughout the whole microstructure of the partially crystallized sealing glass. The microstructure of the sample treated with 0.7 V in Fig. 15a only shows small pores and good adhesion to the metallic substrates. In contrast, the microstructure of the sample treated with 30 V shown in Fig. 15b contains large pores and sufficient leak tightness of the model sealing is no longer given. This is supported by the results of the helium leakage measurements in Table 3. It has to be mentioned that the formation of large pores in the microstructure of the glasses at high voltages is observed reproducibly with various sealing glasses and is not limited to certain components. Up to now no clear explanation can be given for this phenomenon. Schilm *et al.* already described a localized accumulation of pores at anodically polarized gold electrodes in contact with sealing glasses [9].

Detailed SEM images of the oppositely polarized glass-to-metal interfaces of cross-sections in Fig. 15a are given in Fig. 16. In contrast to the composition S01, interfacial layers with a thickness of less than 1 μm are formed at both anodically and cathodically polarized interfaces. No formation of additional silica crystals is observed at anodically polarized interfaces (Fig. 16a.). It seems that only the initially formed $(CrMn)_3O_4$ layer on the metal surface is dissolved into the glass and has formed a thin scale with a composition different to that of the original glass ceramic. Additionally, no migration of oxide particles is

observed. However, the distribution of cristobalite shows a shift towards anodically polarized interface after heat treatment under additional voltage of 0.7 V. In comparison to the main fraction of the visible microstructure, considerably less cristobalite is located in the region near cathodically polarized interfaces. At cathodically polarized glass-to-metal interfaces virtually no interfacial layers can be detected (Fig. 16b). It can be assumed that the initially formed oxide scale on Crofer 22 APU has been dissolved in the glass during the experiment and the cations (Cr, Mn) have migrated and diluted into the glassy phase. This may explain the lack of an interfacial oxide scale at this side. In contrast to this, the presence of ZnO in the standard glass S01 promotes the formation of a distinct oxide scale at cathodically polarized glass-to-metal interfaces (Fig. 11). Thus, the microstructural analysis of model samples of the sealing glass S02 confirms the electrical measurements performed with an applied voltage of 0.7 V. The absence of interfacial layers can be taken as the reason for the non-degrading electrical insulation properties of the sealing glass S02. However, the application of large potentials also leads to the destruction of the sealing glass itself and also of the Crofer 22 APU substrates.

Table 3: Results of measurements of helium leakage rates from model sealings containing the sealing glass S02 which are exposed to dual atmosphere at 850 °C for 300 h.

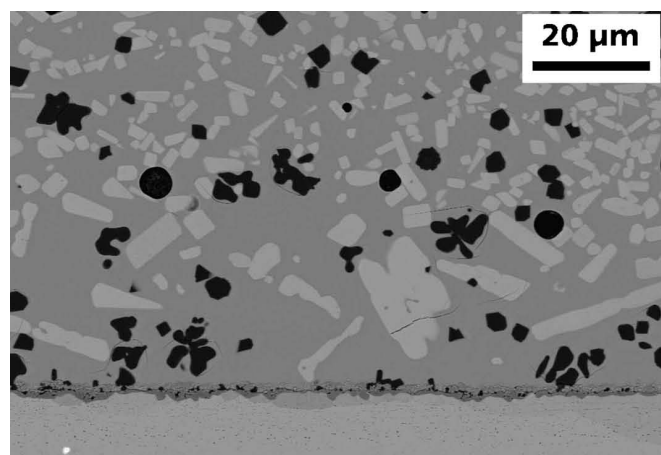| Sample	Applied potential/V	Helium leakage rate/ l mbar s^{-1} cm^{-1}
S02_1	0.7	< 8.3·10^{-11}
S02_2	0.7	< 8.3·10^{-11}
S02_3	30	0.8
S02_4	30	0.8
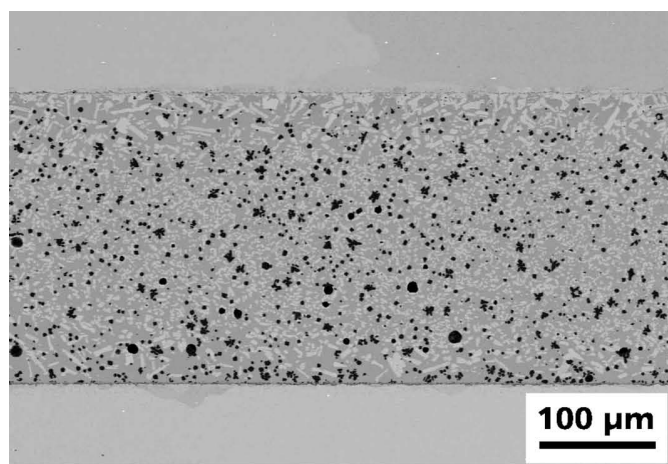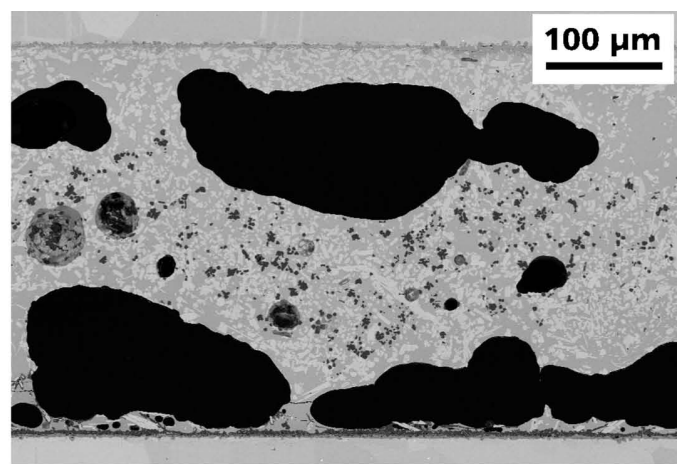
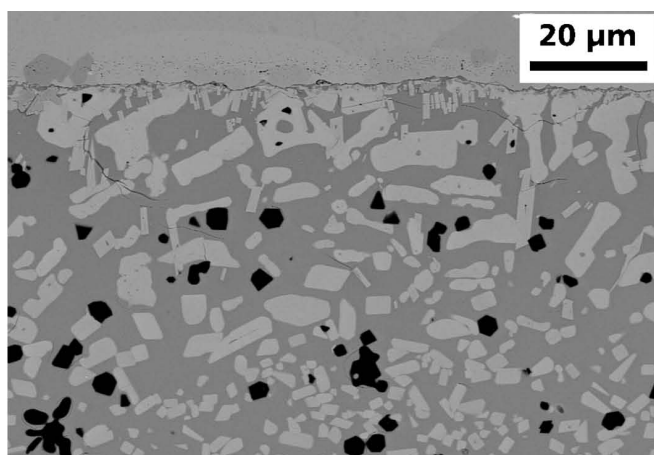a.: U = 0.7 V   b.: U = 30 V

Fig. 15: Microstructure of model sealings containing the sealing glass S02 in contact with Crofer 22 APU substrates after exposure to dual atmosphere for 300 h at 850 °C with applied voltages of 0.7 V (a) and 30 V (b).

a. Anodically polarized interface

b. Cathodically polarized interface

Fig. 16: Microstructure of a model sealing containing the sealing glass S02 in contact with Crofer 22 APU substrates exposure to dual atmosphere for 300 h at 850 °C and a voltage of 0.7 V.

IV. Conclusions

A series of partially crystallizing sealing glasses suitable for joining planar SOFC stacks based on Crofer 22 APU were prepared and characterized in terms of their intrinsic properties and tested in model sealings under conditions that are typical for the operation of SOFCs. Owing to the fact that only one crystalline phase, $BaSi_2O_5$, determines the final properties of the glass ceramics in the sealed state it is possible to exchange components of the residual glassy phase without significantly affecting the relevant sealing properties.

In order to adjust the crystallization properties of the glass ceramics to the sealing process, additional components such as ZnO or alternative oxides are necessary which do not participate in crystallization processes. Simple model glasses without additives crystallize before appropriate sealing conditions are reached, and joints with bad adhesion and insufficient gas tightness are obtained. Investigations of glass seals in sandwich-type model sealings with metallic interconnectors were performed under simulated SOFC operating conditions. The resistivity of the samples was measured *in situ* and values for the resistivity were calculated. ZnO-containing glasses showed considerable degradation in conjunction with SEM investigations of glass-to-metal interfacial layers. The application of d.c. potentials to the model sealings leads to localization of interfacial reactions depending on the anodic or cathodic polarization. These interfacial layers grow with prolonged aging times at high temperatures as well as with increased voltage. The effect of voltage on the resistivities of sealed arrangements strongly depends on the level. While low potentials only affect reactions at the glass-to-metal interfaces, high electric potentials additionally lead to severe destruction of the glass structure at the glass-to-metal interfaces and also of the bulk glass structure itself owing the formation of pores. Particularly ZnO was found to be the most reactive component of the glass ceramic seals involved in degradation processes. An optimized composition of the sealing glasses was developed by replacing ZnO with appropriate oxides. The formation of reaction layers at the glass-to-metal interfaces is minimized, and as a consequence the optimized sealing glasses show constant resistivity on a high level without significant degradation. In summary it can be stated that the development of long-term stable sealing glasses has to be conducted with the support of testing methods that simulate the operating conditions of SOFC. This is necessary in order to recognize degradation processes early and identify critical components and properties of the applied sealing glasses.

References

[1] Zhenguo, Y., Weil K.S., Meinhardt, K.D., Paxton, D.M., Stevenson, J.W.: Considerations of glass sealing SOFC stacks, *Proceedings of the International Conference on Joining of Advanced and Specialty Materials*, **5**, 40 – 46, Columbus, OH, USA, (2002).

[2] Bouche, J.-B., Tietz, F., Sebold, D., Gross, S.M., Koppitz, T., Stöver, D.: Nucleation and crystal growth kinetics of glass-ceramics in the BaO-CaO-Al₂O₃-SiO₂-B₂O₃ system, 7th European SOFC Forum Poster Presentations, (2006).

[3] Smeacetto, F., Salvo, M., Ferraris, M., Cho, J., Boccaccini, A.R: Glass-ceramic seal to join crofer 22 APU alloy to YSZ ceramic in planar SOFCs, *J. Eur. Ceram. Soc.*, **28**, [1], 61 – 68, (2007).

[4] Eichler, K., Kusnecov, M., Jaenicke-Rössler, K., Otschik, P.: Glass foils as sealing elements in SOFC stacks, 6th European Fuel Cell Forum Proceedings, **2**, 792 – 799, Lucerne, (2004).

[5] Meinhardt, K.D., Kim, D.S., Chou, Y.S., Weil, K.S.: Synthesis and properties of a barium aluminosilicate solid oxide fuel cell glass-ceramic sealant, *J. Power Sources*, **182** [2], 188 – 196, (2008).

[6] Gruener, G., De Sousa Meneses, D., Odier, P., Loup, J.P.: Influence of the network on conductivity in ternary CaO-Al₂O₃-SiO₂ glasses and melts, *J. Non-Cryst. Solids*, **281**, [1 – 3], 117 – 124, (2001).

[7] Smeacetto, F., Salvo, M., Ferraris, M., Cho, J., Boccaccini, A.R.: Glass-ceramic seal to join crofer 22 APU alloy to YSZ ceramic in planar SOFCs, *J. Eur. Ceram. Soc.*, **28**, [1], 61 – 68, (2007).

[8] Haanappel, V.A.C., Batfalsky, P., Malzbender, J., Shemet, V., Vinke, I.C., Steinbrech, R.W.: Chemical interaction between glass-ceramic sealants and interconnect steels in SOFC stacks, *J. Power Sources*, **155**, [2], 128 – 137, (2006).

9   Schilm, J., Rost, A., Kusnezoff, M., Michaelis, A.: Sealing glasses for SOFC - degradation behaviour, *Ceram. Eng. Sci. Proc.*, **30**, [4] 185 – 193, (2010).

10 Scholze, H.: Influence of viscosity and surface tension on hot stage microscopy measurements on glasses (in German), *Ber. Dtsch. Keram. Ges.*, **391**, 63 – 68, (1962).

11 Pascual, M.J., Pascual, L., Durán A.: Determination of the viscosity-temperature curve for glasses on the basis of fixed viscosity points determined by hot stage microscopy, *Phys. Chem. Glasses*, **42**, [1], 61 – 66, (2001).

12 Lara, C., Pascual, M.J., Prado, M.O., Durán A.: Sintering of glasses in the system RO-Al$_2$O$_3$-BaO-SiO$_2$ (R=Ca, Mg, Zn) studied by hot-stage microscopy, *Solid State Ionics*, **170**, 201 – 208, (2004).

13 Eberstein, M., Reinsch, S., Müller, R., Deubener, J., Schiller, W.A.: Sintering of glass matrix composites with small rigid inclusions, *J. Eur. Ceram. Soc.*, **29**, 2469 – 2479, (2009).

14 Capoglue, A., Messer, P.F.: Crystallisation behaviour of glass-ceramic coatings based on barium disilicate, *Brit. Cer. Pr.*, **54**, 181 – 187, (1995).

15 Malki, M., Echegut, P.: Electrical conductivity of the CaO-SiO$_2$ system in the solid and the molten states, *J. Non-Cryst. Solids*, **323** [1 – 3], 131 – 136, (2003).

16 Lara, C., Pascual, M.J., Keding, R., Durán, A.: Electrical behaviour of glass ceramics in the systems RO-BaO-SiO$_2$ (R = Mg, Zn) for sealing SOFC, *J. Power Sources*, **157**, 377 – 384, (2006).

17 Pfeiffer, T.: Viscosities and electrical conductivities of oxidic glass-forming melts, *Solid State Ionics*, **105**, [1 – 4], 277 – 287, (1998).

18 Rost, A., Schilm, J., Kusnezoff, M.: Influence of electrical load on the stability of glass sealings, *ECS Transactions*, **25**, [2], 1509 – 1518, (2009).

19 Megel, S.: Cathodic Conduction in Planar Solid Oxide Fuel Cells (in German), Thesis, ISBN 978 – 3-8396 – 0066 – 5, Band 6 Schriftenreihe Kompetenzen in Keramik, Fraunhofer Verlag, Stuttgart, Deutschland, (2009).